

Study structural, surface morphological and magnetic properties of $Mn_{(1-x)}Zn_xFe_2O_4$ by solid state reaction method

Abdulsamee Fawzi AbdulAziz , Kalf Abraheem Kalaiel , Maamar Abdul Aziz Kamil

Natural Ressources Research Center , Tikrit University , Tikrit , Iraq

abdulsamee_fawzi@yahoo.com

Abstract

The powder of Mn-Zn ferrite having the chemical formula $Mn_{(1-x)}Zn_xFe_2O_4$ where x varies from 0, 0.1, 0.2, 0.3, 0.4, and 0.5 were synthesized by solid state Reaction method. The X-Ray Diffraction studies confirm the formation of spinel cubic structure. The particle size was calculated by X-ray broadening studies. Also the structural parameters like Lattice Constant, X-ray density, bulk density (d), Porosity (P), ionic radius (R_a , R_b) and anion parameter or the oxygen positional parameter for all the samples. The micro structural features of the samples were obtained using a Scanning Electron Microscopy (SEM). The magnetic properties of $Mn_{(1-x)}Zn_xFe_2O_4$ ferrites were strongly affected by the Zn content. The saturation magnetization increased. It may be due to relatively high orbital contribution of Mn^{2+} ions to magnetic moment, which gives large induced anisotropy.

Key words: Mn-Zn ferrites, X-ray diffraction, magnetic properties.

Introduction

The Mn – Zn ferrite is a soft ferrite having low magnetic coercivity and high electrical resistivity. These characterizations make these ferrite excellent core materials for power transformers in electric and telecommunication applications [1]. The Mn-Zn ferrites are commonly produced by conventional ceramic processes involving high temperature ($\geq 1200^\circ C$), solid state reactions between the constituent oxides/carbonates. The electronic structure of this material may be qualitatively understood as a generalized Mott insulator [2]. The strong intra-site coulomb repulsion between d electrons splits the partially filled d band into upper and lower Hubbard bands, which results in an insulating electronic ground state and local magnetic moments at the same time [3]. Manganese ferrite ($MnFe_2O_4$) with an inverse spinel structure shows ferrimagnetisms that originates from magnetic moment of anti-parallel spins between Fe^{3+} ions at tetrahedral sites Mn^{2+} ions at octahedral sites [4]. Morrison et al [5] has observed the presence of Zn^{2+} ions in octahedral sites in the as prepared state itself when the material was prepared with 7nm size particle using reverse micelle process. The present work aims to carry out multifold studies in a comprehensive manner.

1. Preparation of $Mn_{(1-x)}Zn_xFe_2O_4$ where x = 0, 0.1, 0.2, 0.3, 0.4 and 0.5 sintered at $1200^\circ C$ are referred as C_1 , C_2 , C_3 , C_4 , C_5 and C_6 by ceramic method.

2. X-Ray Diffraction studies to confirm the constituent phase formation. This technique is also used to study the structural deformation of phase by calculating lattice parameters.

3. Surface morphological studies by SEM.

Experimental details

The Mn-Zn ferrites were prepared using the Ceramic route. The powders of MnO, ZnO and Fe_2O_3 in the required stoichiometry were thoroughly mixed of oxides as required for final product. The second stage of pre-sintering involves heating of intimate

mixture of raw materials in order to decompose carbonates and higher oxides. The pre-sintering helps in homogenization, to remove the absorbed gases and moisture, causes partial reaction of the oxides and tends to reduce the shrinkage during the final sintering. The pre-sintered powder is then ground to fine powder to reduce the particle size and to promote mixing of any unreacted oxides. The dried powder is pressed to the required shape using the binder 1% polyvinyl alcohol in adie, applying pressure of 5-6 tons by means of hydraulic press. The pellets of the required shape are thus formed for further processing. The final stage of sintering involves heating the pressed material unnecessary at $1200^\circ C$ for 12 hours. The sintering involves large scale diffusion and erasing of gradients of chemical potentials, resulting in information of product.

The single phase formation of the materials was confirmed by powder X-ray diffraction technique. X-ray diffractogram of all samples was recorded using an X-ray diffractometer (model Bruker D8 Advance). The X-ray diffractograms were obtained using Cu $K\alpha$ radiation on a Philips X-ray diffractometer (model PW1710). The diffraction patterns show the sharp lines corresponding to a single-phase spinel structure for all the samples. The SEM micrograph studies were carried using SEM model JEOL JSM 6360. The magnetization measurements studies were carried out by using the high field hysteresis loop tracer designed at department of physics, pune university, Pune-India.

Results and discussion:-

Structural analysis by XRD

X-ray diffraction patterns for $Mn_{1-x}Zn_xFe_2O_4$ sintered at $1200^\circ C$ are shown in Fig. 1. The X-ray patterns show the existence of spinel structure with the reflection planes (220), (311), (222), (400), (422), (511), (440) and (533). It is found that for the samples sintered at $1200^\circ C$, the single phase spinel structure

was constructed. There are no extra peaks indicating purity of the samples synthesized. The positions of all the Bragg lines were used to obtain the interplaner spacing and these values were used to index the peaks. The observed and calculated (d) values are given in table (1). These values are in good agreement with each other for all indexed planes in case of all samples. The lattice constant (a) and the Miller indices (hkl) of reflecting planes are related by the following equation [6].

$$d = \frac{a}{\sqrt{h^2 + k^2 + l^2}} \text{----- (1)}$$

Substituting the values of (d) in equation (1) one can calculate the lattice parameter (a).

The average particle size (D_p) of the samples is calculated using Scherrer's equation [7].

$$D_p = \frac{k\lambda}{\beta \cos\theta} \text{----- (2)}$$

where $k = 0.89$ (assuming the particles are spherical in shape); $\lambda =$ wavelength of X-ray; $\beta =$ full width at half maximum (FWHM) of the diffraction peak; and $\theta =$ angle of diffraction. The X-ray density of the ferrite and ferroelectric was calculated using the following formula [8]:

$$\rho_1 = 8M / Na^3 \text{----- (3)}$$

where, M is the molecular weight expressed in grams, (a) is the lattice constant and N is Avogadro's number (6.023×10^{23} molecule / mole).

The actual density of the samples can be calculated using the Hendrick and Adams method [9]. This method depends upon the weight of the sample in air and in a liquid of known density in which the sample

is insoluble. In the present studies xylene was used as liquid in which ferrite/ ferroelectric/ composite sample were immersed. For these samples xylenes ($\rho = 0.861 \text{ g/cm}^3$ at 20°C) was used. The actual density (ρ_a) was calculated using the formula

$$\rho_a = \frac{\text{Weight of sample in air}}{\text{Weight of sample in air} - \text{Weight in xylene}} \times \text{density of xylene} \text{---- (4)}$$

$$\rho_a = \frac{W_{air}}{W_{air} - W_{Liquid}} \times \rho_{Xylene}$$

The porosity was calculated by using the following equation [10].

$$\text{Percentage porosity} = \left\{ \frac{100(\rho - \rho_a)}{\rho_x} \right\} \% \text{---- (5)}$$

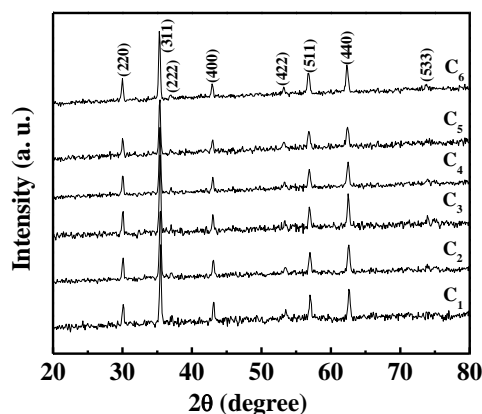


Fig. 1 X- ray diffraction patterns of C₁, C₂, C₃, C₄, C₅ and C₆ samples.

Table 1 Miller indices and inter planer spacing for Mn_(1-x)Zn_xFe₂O₄ ferrites.

(hkl)	d _{std.}	C ₁	C ₂	C ₃	C ₄	C ₅	C ₆
		d _{obs.}					
(220)	2.966	2.970	2.970	2.970	2.980	2.980	2.980
(311)	2.531	2.529	2.528	2.530	2.532	2.534	2.535
(222)	2.424	2.424	2.424	2.431	2.430	2.437	2.430
(400)	2.099	2.099	2.099	2.104	2.104	2.104	2.109
(422)	1.713	1.713	1.713	1.716	1.719	1.722	1.722
(511)	1.615	1.616	1.616	1.618	1.618	1.621	1.621
(440)	1.483	1.484	1.484	1.486	1.486	1.488	1.490
(533)	1.279	1.284	1.283	1.283	1.283	1.284	1.284

The variation in values of lattice constant, effective crystallize size, lattice strain, X-ray density, bond lengths, ionic radius per molecule of the tetrahedral and octahedral sites and oxygen position parameter for all series have been calculated in a same fashion to that of Mn-Zn ferrite system are given in table 2 . It is clear from table 2 that with increase in Zn concentration in place of manganese the lattice parameter increases. The linear increase in the lattice constant is due to the replacement of Zn²⁺ (0.74 Å) ions by larger Zn²⁺ ions with an ionic radius of Mn²⁺ (0.83 Å) in the system Mn_(1-x)Zn_xFe₂O₄. Similar results are obtained for Co-Zn ferrite system [11]

In ferrites, the charge carriers are not completely free but are strongly localized in the d-shell; this localization may be due to formation of polarons. A small polaron defect is created when an electronic carrier gets trapped at given sites as a consequence of the displacement of adjacent atoms or ions. An attempt has been made to calculate the polaron radius for all the samples studied by using the following relation [12].

$$r_p = \frac{1}{2} \left[\frac{\pi}{6N'} \right]^{1/3} \text{----- (6)}$$

where N' number of sites per unit volume = $96/a^3$. Also we have calculated jump length (L) by using the following relation [13].

$$L = a\sqrt{2}/4 \text{ ----- (7)}$$

The values of jump length for various values of Zn concentration are summarized in Table 2. This shows that Jump length (L) and polaron radius (r_p) increases with increasing Zn concentration suggests that charge carriers require more energy to jump from one

cationic site to other. Theoretical density obtained from X-ray diffraction data and experimental density obtained using Archimedes principle was used to obtain porosity in the samples. It is seen from the Table 2 that the porosity decreases with increase in Zn concentration. The decrease in porosity is due to larger ionic radii of Mn^{2+} as compared to Zn^{2+} . This may be due to evaporation of Zn^{2+} ions at higher sintering temperature.

Table 2 lattice constant (a), effective crystallite size (ϵ), lattice strain (η), polaron radius (r_p) Jump rate (L), x-ray density (ρ_x), actual density (ρ_a) and percentage porosity (p).

Sample	A (Å)	ϵ (nm)	η (%)	r_p (Å)	L(Å)	ρ_x (gm/cm ³)	ρ_a (gm/cm ³)	P(%)
C ₁	8.499	21.9	2.8×10^{-3}	0.738	2.966	5.210	4.880	6.334
C ₂	8.489	25.1	2.8×10^{-3}	0.739	2.970	5.213	4.929	5.450
C ₃	8.480	22.2	2.9×10^{-3}	0.740	2.974	5.214	4.976	4.564
C ₄	8.371	21.4	2.8×10^{-3}	0.740	2.978	5.215	5.025	3.643
C ₅	8.460	22.2	2.8×10^{-3}	0.741	2.980	5.217	5.107	2.108
C ₆	8.451	22.2	2.9×10^{-3}	0.742	2.986	5.218	5.121	1.850

The variation in values of bond lengths, ionic radius per molecule of the tetrahedral and octahedral sites and oxygen position parameter for all series have been calculated in a same fashion to that of Mn-Zn ferrite system are given in table 3. It can be seen that the mean tetrahedral ionic radius increases continuously with increasing Zn-concentration. It is observed that ionic radius of the octahedral site decreases with increasing Zn concentration. As such, it can be concluded that in the present system tetrahedral site substitution plays a dominant role in influencing the value of the lattice constant. The Bond lengths R_A and R_B are calculated by using the equations (8) and (9) respectively.

$$R_A = (u - 1/4)a\sqrt{3} \text{ (8)}$$

$$R_B = (5/8 - u)a \text{ (9)}$$

where $u = 0.381$ is oxygen parameter for nickel ferrite[14]

The oxygen positional parameter or anion parameter (u) for each composition was calculated by using the following formula [15], and is given in table 1.

$$u^{3m} = \frac{\frac{1}{4}R^2 - \frac{2}{3} + \left[\frac{11}{48}R^2 - \frac{1}{18} \right]^{1/2}}{2R^2 - 2} \text{ .. (10)}$$

where $R = R_B/R_A$.. The bond lengths R_B , R_A are average bond lengths,

Table 3 Cation distribution, bond lengths (R_A , R_B), ionic radius per molecule of the tetrahedral and octahedral sites (r_A , r_B) and oxygen position parameter (u)

Samples	Substance	Tetrahedral A sites	Tetrahedral B sites	R_A (Å)	R_B (Å)	r_A (Å)	r_B (Å)	u(Å)
C ₁	MnO.Fe ₂ O ₃	Fe ³⁺	Mn ²⁺ .Fe ³⁺	1.990	2.045	0.67	0.725	0.2600
C ₂	0.9MnO.Fe ₂ O ₃ 0.1ZnO.Fe ₂ O ₃	Zn ²⁺ _{0.1} Fe ³⁺ _{0.9}	Mn ²⁺ _{0.9} .Fe ³⁺ _{1.1}	2.006	2.039	0.686	0.719	0.2610
C ₃	0.8MnO.Fe ₂ O ₃ 0.2ZnO.Fe ₂ O ₃	Zn ²⁺ _{0.2} Fe ³⁺ _{0.8}	Mn ²⁺ _{0.8} .Fe ³⁺ _{1.2}	2.022	2.034	0.702	0.714	0.2619
C ₄	0.7MnO.Fe ₂ O ₃ 0.3ZnO.Fe ₂ O ₃	Zn ²⁺ _{0.3} Fe ³⁺ _{0.7}	Mn ²⁺ _{0.7} .Fe ³⁺ _{1.3}	2.038	2.028	0.718	0.708	0.2629
C ₅	0.6MnO.Fe ₂ O ₃ 0.4ZnO.Fe ₂ O ₃	Zn ²⁺ _{0.4} Fe ³⁺ _{0.6}	Mn ²⁺ _{0.6} .Fe ³⁺ _{1.4}	2.054	2.023	0.734	0.703	0.2638
C ₆	0.5MnO.Fe ₂ O ₃ 0.5ZnO.Fe ₂ O ₃	Zn ²⁺ _{0.5} Fe ³⁺ _{0.5}	Mn ²⁺ _{0.5} .Fe ³⁺ _{1.5}	2.070	2.017	0.750	0.697	0.2648

Surface Morphological studies by SEM

Fig. 2 show micrographs of the samples C₁ – C₆ sintered at 1200 °C. It is seen from the micrographs that the grains are well compacted with wide size distribution. The grains are polygonal in shape and

size goes on increasing with increasing Zn concentration. The increase in grain size with increase in Zn concentration is attributed to higher reactivity of Zn^{2+} .

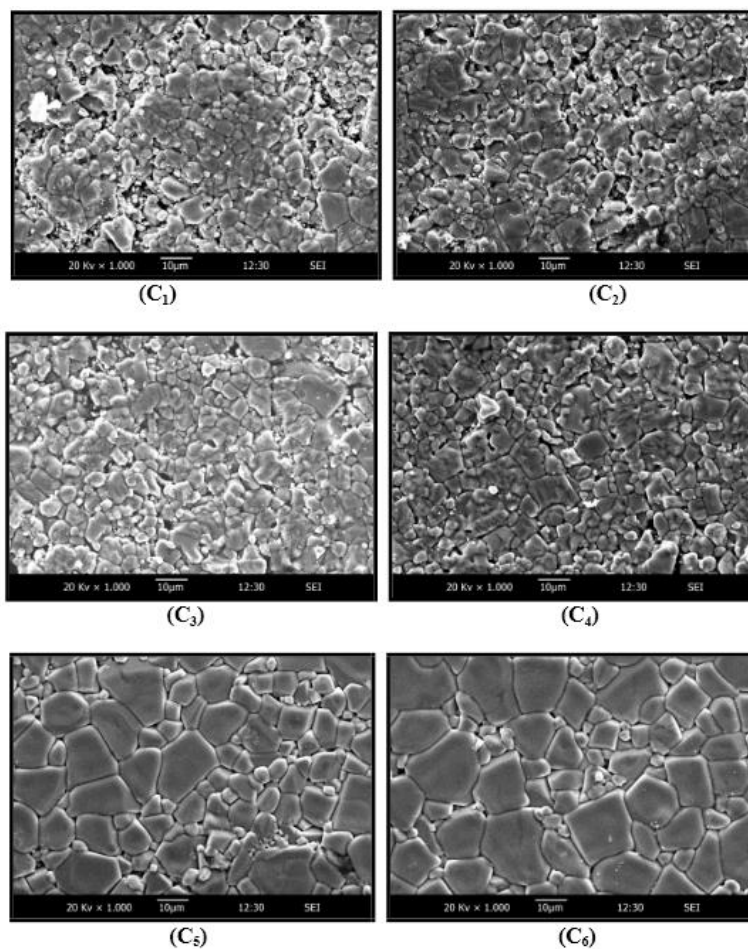


Fig. 2 SEM micrograph of C₁, C₂, C₃, C₄, C₅ and C₆ samples.

Magnetic Hysteresis

Magnetic hysteresis plots for C₁, C₂, C₃, C₄, C₅ and C₆ samples are shown in Fig.3. The main observations from Fig.3. Are as follows: i) All the plots show magnetic hysteresis behavior at room temperature. The magnetic field at which saturation magnetization increases from 2000 gauss to 5000 gauss as Zn content in place of Mn in MnFe₂O₄ increases. ii) All the samples under study show clear saturation of magnetization. The saturation magnetization increases with increase in Zn²⁺ content in place of Mn²⁺ in MnFe₂O₄ increases. The increase in saturation magnetization may be primarily due to the substitution of nonmagnetic Zn²⁺ ion (d¹⁰) for Mn²⁺ into the magnetic ferrite lattice. Zn²⁺ has a stronger preference for the tetrahedral site (A site), while Mn²⁺ ions (for which Zn is substituted) are located on octahedral site (B site) of AB₂O₄ spinel ferrite. Thus, Zn²⁺ displaces Fe³⁺ from A to B site. As the magnetic spin of neighboring A and B sites are anti-ferromagnetically coupled (due to the super exchange interaction in ferrite lattice), the net result is an increase in magnetic moment on B sub-lattice, as well as the increase of the net magnetic moment of the crystal [16]. Cation distribution and net moment per Molecule of Mn_(1-x)Zn_xFe₂O₄ samples can be

explained and is given schematically in the following table 4. It shows how the calculation is made for Mn-Zn ferrite samples. The structure is inverse, with all the Mn²⁺ moments of the Fe³⁺ ions therefore cancel, and the net moment is simply that of the Mn² ions in B site and the Fe³⁺ ions evenly between A and B site while Zn²⁺ ions non magnetic, which is 0 μ_B Occupy the A- sites [17]. Generalizing on this, we conclude that the the saturation magnetization μ_H of any inverse ferrite is simply the moment on the divalent ion.

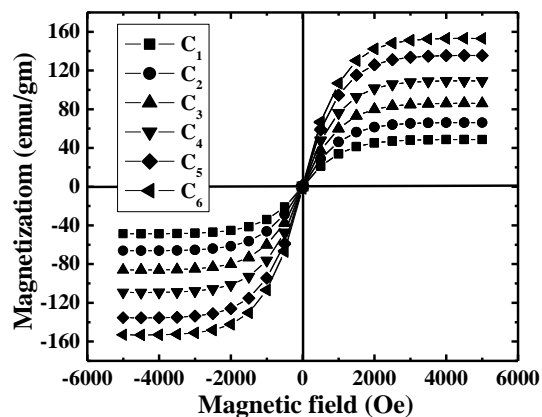


Fig. 3 Hysteresis of C₁, C₂, C₃, C₄, C₅ and C₆ samples.

Table 4: Cation distribution and net moment per Molecule of $Mn_{(1-x)}Zn_xFe_2O_4$ samples.

Samples	Substance	Structure	Tetrahedral A Site	Octrahedral B Site	Net Moment (μB /Molecule)
C ₁	MnO.Fe ₂ O ₃	Inverse	Fe ³⁺ 5	Mn ²⁺ Fe ³⁺ 5 5	5
C ₂	0.9Mn.Fe ₂ O ₃	Inverse	Fe ³⁺ 4.5	Mn ²⁺ Fe ³⁺ 4.5 4.5	4.5
	0.1ZnO.Fe ₂ O ₃	Normal	Zn ²⁺ 0	Fe ³⁺ Fe ³⁺ 0.5 0.5	1 — 5.5
C ₃	0.8MnO.Fe ₂ O ₃	Inverse	Fe ³⁺ 4	Mn ²⁺ Fe ³⁺ 4 4	4
	0.2ZnO.Fe ₂ O ₃	Normal	Zn ²⁺ 0	Fe ³⁺ Fe ³⁺ 1 1	2 — 6
C ₄	0.7MnO.Fe ₂ O ₃	Inverse	Fe ³⁺ 3.5	Mn ²⁺ Fe ³⁺ 3.5 3.5	3.5
	0.3ZnO.Fe ₂ O ₃	Normal	Zn ²⁺ 0	Fe ³⁺ Fe ³⁺ 1.5 1.5	3 — 6.5
C ₅	0.6MnO.Fe ₂ O ₃	Inverse	Fe ³⁺ 3	Mn ²⁺ Fe ³⁺ 3 3	3
	0.4ZnO.Fe ₂ O ₃	Normal	Zn ²⁺ 0	Fe ³⁺ Fe ³⁺ 2 2	4 — 7
C ₆	0.5MnO.Fe ₂ O ₃	Inverse	Fe ³⁺ 2.5	Mn ²⁺ Fe ³⁺ 2.5 2.5	2.5
	0.5ZnO.Fe ₂ O ₃	Normal	Zn ²⁺ 0	Fe ³⁺ Fe ³⁺ 2.5 2.5	5 — 7.5

Conclusions

In the present work, we have successfully synthesized $Mn_{1-x}Zn_xFe_2O_4$ ferrites by solid state reaction method. In the structural study of Mn-Zn ferrites, crystalline nature is confirmed by X-ray diffraction. The Bragg's peaks observed in XRD plots are matching with the JCPDS data which indicates that the materials formed are of single phase having inverse spinel cubic structure. Also lattice constant, unit cell volume, X-ray density, bulk density, porosity, pore fraction, ionic radius and anion parameter or the oxygen

References

- [1] T. Abraham, J. Am. Ceramic. Soc. Bull. 73 (1994) 62.
- [2] N. F. Mott Proc. Phys. Sco. London 49 (1937) 72.
- [3] N. F. Mott, Phil. Mag. 6 (1961) 287.
- [4] D. S. Erickson, J. O. Mason, J. Solid St. Chem. 59 (1985) 42.
- [5] S. A. Morrison, C. L. Cahill, E. E. Carpenter, S. Calvin, R Swaminathan and McHenry M E, V. G. Harris, J. Appl. Phys. 95 (2004) 6392.
- [6] V. Raghavan, "Materials Science and Engineering" (2006).

positional parameter for all the samples are determined from XRD which agree with the theoretical data. The scanning electron micrographs of the Mn-Zn ferrites show that the grains are nearly homogeneous and uniformly distributed in the samples. The observation of magnetic hysteresis loop at room temperature confirms existence of ferroelectric and magnetic ordering simultaneously at room temperature for all samples. The saturation magnetization increases with increase on Zn content.

- [7] C. Hammond, "The Basic of Crystallography and Diffraction" Oxford University Press, Oxford (2001).
- [8] C. Duran, S. T. McKinstry and G. L. Messing. J. Electroceram. 10 (2003) 47.
- [9] Xiwei Qi, Ji Zhou, Baorang Li, Yingchun Zhang, Zhenxing Yue, Zhilun Gui, and Longtu Li, J. Am. Ceram. Soc., 87 (2004) 1848.
- [10] A. D. Sheikh and V. L. Mathe., J. Mater. Sci. 43 (2008) 2018.
- [11] A.M. Abdeen, O.M. Hemeda, E.E. Assem, M.M. El-Sehly, Journal of Magnetism and Magnetic Materials 238 (2002) 75–83.

- [12] A. J. Bosman and J. H. Van Dall. Adv. Phys: 1(1970) 19.
 [13] B. Gillot and F. Jemmali, Phys. Stat. Sol. (a) 76 (1983) 601.
 [14] N. H. Vasoya, V. K. Lakhani, P. U. Sharma, K. B. Modi, Ravi Kumar and H. H. Joshi J. Phys.: Condens. Matter 18 (2006) 8063.
 [15] M. Z. Said, D. M. Hemed, S. A. Kader and G. Z. Farag, Turk J. Phys, 30 (2006)1-10.
 [16] M. Mallapur, M. Phil. Dissertation, Shivaji Univ., Kolhapur (2003).
 [17] B C. Cullity and C. D. Graham, "Introduction to magnetoelectric materials" (2009)

" دراسة الخواص التركيبية؛ ومورفولوجية السطح والخواص المغناطيسية لمركبات $Mn_{(1-x)}Zn_x$

Fe_2O_4 المحضرة بطريقة تفاعلات الحالة الصلبة"

عبدالسميع فوزي عبدالعزيز ، خلف ابراهيم خليل ، معمر عبدالعزيز كامل

مركز بحوث الموارد الطبيعية ، جامعة تكريت ، تكريت ، العراق

الملخص

تم تحضير مركبات المنغنيز - خارصين ذات الصيغة الكيميائية $Mn_{(1-x)}Zn_xFe_2O_4$ حيث $0 \leq x \leq 0.5$ وذلك باستخدام طريقة تفاعلات الحالة الصلبة. تم حساب الحجم الحبيبي لجميع مركبات الفرايت المحضرة من حيود الأشعة السينية بعد التأكد من تشكيل الطور الأحادي ذو التركيب البلوري مغزلي الشكل. كما تم حساب ثابت الشبكة والكثافة الظاهرية المحسوبة من حيود الأشعة السينية (ρ_{x-ray}) ، والكثافة الفيزيائية، ونصف القطر الايوني حيث وجد أنها تزداد مع زيادة تركيز نسبة خارصين، بينما كانت المسامية تنقص مع زيادة تركيز الكاديوم. كما لوحظ صور التركيب الميكروي لجميع النماذج بواسطة مجهر الماسح الالكتروني. أما نتائج الفحوصات المغناطيسية فقد أظهرت تأثير نسبة خارصين على زيادة المغناطيسية المشبعة. قد تكون نتيجة المساهمة النسبية للقيمة العالية لاوربيثال العزم المغناطيسي لايون المنغنيز الذي يسبب زيادة الخواص المتباينة.

الكلمات الافتتاحية: منغنيز - خارصين فيرايت، حيود الاشعة السينية، الخواص المغناطيسية